Dynamics and transport in mean-field coupled, many degrees-of-freedom, area-preserving nontwist maps.

L. Carbajal
Institute of Nuclear Sciences, Universidad Nacional Autónoma de México

D. del-Castillo-Negrete
Oak Ridge National Laboratory, Oak Ridge, Tennessee, USA

J. J. Martinell
Institute of Nuclear Sciences, Universidad Nacional Autónoma de México.
(Dated: February 23, 2012)

Area-preserving nontwist maps, i.e. maps that violate the twist condition, arise in the study of degenerate Hamiltonian systems for which the standard version of the KAM theorem fails to apply. These maps have found applications in several areas including plasma physics, fluid mechanics, and condensed matter physics. Previous work has limited attention to maps in 2-dimensional phase space. Going beyond these studies, in this paper we study nontwist maps with many-degrees-of-freedom. We propose a model in which the different degrees of freedom are coupled through a mean-field that evolves self-consistently. Based on the linear stability of period-one and period-two orbits of the coupled maps, we construct coherent states in which the degrees of freedom are synchronized and the mean-field stays nearly fixed. Nontwist systems exhibit global bifurcations in phase space known as separatrix reconnection. Here we show that the mean-field coupling leads to dynamic, self-consistent reconnection in which transport across invariant curves can take place in the absence of chaos due to changes in the topology of the separatrices. In the context of self-consistent chaotic transport we study two novel problems: suppression of diffusion and breakup of the shearless curve. For both problems we construct a macroscopic effective diffusion model with time-dependent diffusivity. Self-consistent transport near criticality is also studied, and it is shown that the threshold for global transport as function of time is a fat-fractal Cantor set.

Nontwist area-preserving maps are discrete representations in time of degenerate Hamiltonians that have found applications in fluid mechanics, plasma physics, atomic physics, and condensed matter physics. These maps are also theoretically interesting because powerful results including the standard KAM theorem, the Poincare-Birkhoff theorem, and the Aubry-Mather theory cannot be applied to them. Two unique features of this type of maps are the existence of robust transport barriers and the possibility of bifurcations of the phase space topology due to separatrix reconnection. As a first step to study these phenomena in the case of many-degrees-of-freedom systems, we study a model of intermediate complexity between the well-understood 2-dimensional area-preserving nontwist maps and the fully coupled $2N$-dimensional many-body system. The proposed model consists of a family of mean-field coupled area-preserving nontwist maps, in which the interaction between the degrees of freedom is mediated by a long-range field whose evolution depends on the mean properties of the system. The coupling is motivated by the generic interaction found in weakly-linear descriptions of plasma and fluid instabilities. Novel results are presented on the formation of coherent structures, nonchaotic global transport due to self-consistent separatrix reconnection, the role of mean-field coupling in diffusive transport, and self-similar scaling of intermittent self-consistent transport near criticality.

I. INTRODUCTION

Area-preserving maps of the form

$$\begin{aligned} x^{n+1} &= x^n + \Omega(y^{n+1}), \\ y^{n+1} &= y^n + f(x^n), \end{aligned} \tag{1}$$

where (x^n, y^n) denotes the n-th iterate of the map, have proved to be very useful in numerical and analytical studies of Hamiltonian chaos in low degrees-of-freedom systems. In particular, the standard map, for which $\Omega = y^{n+1}$, and $f = \kappa \sin(x^n - \theta)$, is a paradigmatic model to study periodically perturbed, chaotic, one-and-a-half degrees-of-freedom systems.

However, compared with the progress made in the study of chaos in low degrees-of-freedom systems, the understanding of Hamiltonian chaos in systems with many degrees-of-freedom is in its infancy. In general, the phase space of N interacting particles in a three-dimensional space, is $6N$-dimensional, and the dynamics is determined by $6N$ nonlinearly coupled, first order, ordinary differential equations. One avenue to approach this challenging problem is throughout the use of mean-field models in which the mutual interaction of the particles is mediated by a global field whose evolution is determined

self-consistently from the particle dynamics. In the context of discrete dynamical systems, this mean-field approach leads to the study of globally coupled maps.

Of particular interest to the present work are the discrete-in-time, mean-field Hamiltonian models proposed in Refs. 1,2. As discussed in Ref. 1, in the case when the coupling involves area-preserving standard maps, the two-dimensional dynamics of an ensemble of N-particles with coordinates (x_k^n, y_k^n), $k = 1, 2, \ldots N$, at time n, evolves according to

$$x_k^{n+1} = x_k^n + y_k^{n+1}, \tag{2}$$
$$y_k^{n+1} = y_k^n - \kappa^{n+1} \sin\left(x_k^n - \theta^n\right), \tag{3}$$

where κ^n and θ^n denote the amplitude and phase of the mean-field, which evolve with n according to

$$\theta^{n+1} = \theta^n + \frac{1}{\kappa^{n+1}} \frac{\partial \eta^n}{\partial \theta^n}, \tag{4}$$
$$\kappa^{n+1} = \sqrt{(\kappa^n)^2 + (\eta^n)^2} + \eta^n, \tag{5}$$

where

$$\eta^n = \sum_{k=1}^{N} \gamma_k \sin(x_k^n - \theta^n), \tag{6}$$

is the mean-field coupling with γ_k constants. In the absence of coupling, $\gamma_k = 0$, each degree of freedom evolves independently following the standard map dynamics with fixed κ and θ.

The mean-field model in Eqs. (2)-(6) is a useful laboratory to explore the dynamics of Hamiltonian systems with a large number of degrees of freedom in the context of area-preserving maps. This model arises from the discretization of the continuous-in-time, Single Wave Model, which is a generic model describing the weakly nonlinear dynamics of kinetic instabilities in plasmas, and shear flow instabilities in fluids. In the plasma physics context, the model describes the nonlinear wave-particle interaction in a Vlasov-Poisson plasma near marginal stability in the weakly nonlinear limit. In this case, (x_k^n, y_k^n) denote the phase space coordinates of an ensemble of electrons interacting self-consistently with an electrostatic, single mode wave with amplitude κ^n and phase θ^n, in a positive, neutralizing ion background. The strength of the coupling is determined by the constants, γ_k, which depend on the relative charge of the particles with respect to the background[1,3]. In fluids, the model provides a simplified description of two-dimensional vortex dynamics in the presence of a strong background shear flow. In this context, (x_k^n, y_k^n) denote the coordinates of an ensemble of point vortices interacting self-consistently with a single-mode shear-flow instability, with the coupling constants γ_k determined by the strength of the vortices[1]. In both, plasmas and fluids, the coupling constants can be positive or negative. As discussed in Ref. 4, the single wave model is also closely related to recent mean-field models used to study the statistical mechanics of long-range interacting systems.

The main goal of the present paper is to formulate and study the analogue of the mean-field model in Eqs. (2)-(6) for the case of nontwist maps. These maps are characterized by the violation of the twist condition, which requires

$$\frac{\partial x^{n+1}}{\partial y^n} \neq 0, \tag{7}$$

for all y^n. Nontwist maps, arise in the study of the transition to chaos in perturbed degenerate Hamiltonian systems. A paradigmatic example is the standard nontwist map

$$x_{n+1} = x_n + a(1 - y_{n+1}^2),$$
$$y_{n+1} = y_n - \kappa \sin\left(x_n - \theta\right). \tag{8}$$

In this map, in the limit $\kappa = 0$, the twist condition is violated along the $y = 0$ line, known as the shearless curve that creates a central transport barrier (CTB). This map was proposed in Ref. 5 as a simplified model to study chaotic transport in geophysical flows and it has also been used to study of transport in magnetically confined plasmas[6–8]. Note that, to simplify the notation, Eq. (8) corresponds to the standard nontwist map in Ref. 10 with the x-coordinated rescaled as $x \to x/(2\pi)$. Nontwist maps are interesting from the point of view of basic Hamiltonian dynamics because the violation of the twist conditions precludes the applications of powerful theorems including the standard KAM theorem, the Poincare-Birkhoff theorem, and the Aubry-Mather theory. This has motivated new mathematical developments including, among others, extensions of KAM theory that do not rely on the validity of the twist condition[9].

Two key aspects of nontwist systems of particular interest to the present study are the robustness of invariant circles, and separatrix reconnection. Previous works have shown that in area-preserving maps of the form in Eq. (8), shearless invariant curves are remarkably resilient to breakup[10,11]. The violation of the twist condition also gives rise to a highly nontrivial changes in the phase space topology generically known as separatrix reconnection see e.g., Refs. 10,12 and references therein. It is thus of significant interest from the dynamical systems point of view to study the roll of mean-field coupling in these phenomena. Our approach to address these problems is based on the study of the nontwist generalization of the coupled map model in Eqs. (2)-(6) obtained by replacing Eq. (2) by

$$x_k^{n+1} = x_k^n + a\left[1 - \left(y_k^{n+1}\right)^2\right]. \tag{9}$$

Throughout this paper, we refer to Eqs. (9) and (3)-(6) as the nontwist mean-field (NTMF) model.

The organization of the rest of the paper is as follows. Section II defines the model using generating functions for generic mean-field couplings. This formal approach is intended to complement the intuitive description presented above. Section II also contains a description of period-one and period-two orbits, and their stability properties. The relationship between the stability

of the periodic orbits and the existence of coherent structures in phase space is also discussed.

Section III studies the role of mean-field coupling in separatrix reconnection. Contrary to the standard nontwist map in Eq. (8), for which the phase space topology is determined by the a priori chosen values of a and κ, in the NTMF map, separatrix reconnection is dynamically determined by the self-consistent interaction of the different degrees of freedom through the mean-field. Of particular interest is the study of dynamic separatrix reconnection leading to transport across the CTB. Section IV is devoted to the study of self-consistent diffusion. We study the role of the mean-field coupling in the suppression of diffusion and in the destruction of the CTB. For both cases, an effective diffusive, quasi-linear model is constructed. Section IV also discusses intermittent transport occurring when the self-consistent evolution of the mean-field brings κ^n near the critical transition point for the destruction of the CTB. Section V presents the conclusions.

II. MODEL DESCRIPTION, PERIODIC ORBITS, AND COHERENT STRUCTURES

The formation of coherent structures is a problem of considerable interest in systems with many degrees-of-freedom systems. In Refs. **?** this problem was addressed in the context of continuous in time Hamiltonian mean-field models in the finite N and $N \to \infty$ limits. In particular, it was shown that the single wave model exhibits dipole coherent structures in phase space in the presence of self-consistent chaos. Here we study coherent structures in the context of the discrete in time NTMF model

The NTMF model describes the evolution of N-degrees of freedom, referred here as "particles", with coordinates $(x_1, \dots x_N)$ in a one-dimensional periodic domain, $x_k \in (0, 2\pi)$, and momenta $(p_1, \dots p_N)$, coupled to an oscillating mean-field with amplitude, J, and phase, θ. Since the system is Hamiltonian, its evolution can be described as a canonical transformation of the form $(\mathbf{q}, \mathbf{p})^n \to (\mathbf{q}, \mathbf{p})^{n+1}$ defined by

$$\mathbf{q}^{n+1} = \frac{\partial S}{\partial \mathbf{p}^{n+1}}\,, \qquad \mathbf{p}^n = \frac{\partial S}{\partial \mathbf{q}^n}\,, \tag{10}$$

where the $N+1$ canonical conjugated coordinates are $\mathbf{q} = (x_1, \dots x_N, \theta)$, and $\mathbf{p} = (p_1, \dots p_N, J)$, and $S = S(\mathbf{q}^n, \mathbf{p}^{n+1})$ is the generating function. Following Ref. 2 we write,

$$S = S_p + S_f + S_i\,, \tag{11}$$

where S_p determines the evolution of the N-particles in the absence of the mean-field; S_f determines the uncoupled evolution of the field; and S_i determines the interaction of the mean-field with the particles. For S_p we use the generating function of the unperturbed standard nontwist map,

$$S_p = \sum_{k=1}^{N} \left\{ x_k^n p_k^{n+1} + a\left[p_k^{n+1} - \frac{1}{3}\frac{\Delta t^2}{\Gamma_k^2}\left(p_k^{n+1}\right)^3 \right] \right\}. \tag{12}$$

In the absence of interaction, the evolution of the mean-field is determined by

$$S_f = \theta^n J^{n+1}\,, \tag{13}$$

while the coupling between the mean-field and the particles is given by

$$S_i = -2\Delta t \sum_{k=1}^{N} \sqrt{J^{n+1}}\Gamma_k \cos(x_k^n - \theta^n)\,, \tag{14}$$

where Δt, Γ_1, $\dots$, Γ_N are constants. Although it is possible, and interesting, to consider maps coupled only through the phases, like in the study of twist maps in Ref. 2, here we focus attention in couplings involving both the amplitude and the phase.

Substituting Eqs. (12)-(14) into (10) we get the $2(N+1)$ symplectic map describing the self-consistent interaction of the N-particles with the mean-field

$$x_k^{n+1} = x_k^n + a\left[1 - \left(\frac{\Delta t}{\Gamma_k} p_k^{n+1}\right)^2\right], \tag{15}$$

$$p_k^{n+1} = p_k^n - 2\Delta t \Gamma_k \sqrt{J^{n+1}} \sin\left(x_k^n - \theta^n\right), \tag{16}$$

$$\theta^{n+1} = \theta^n - U\Delta t - \frac{\Delta t}{\sqrt{J^{n+1}}} \sum_{k=1}^{N} \Gamma_k \cos\left(x_k^n - \theta^n\right), \tag{17}$$

$$J^{n+1} = J^n + 2\Delta t \sqrt{J^{n+1}} \sum_{k=1}^{N} \Gamma_k \sin\left(x_k^n - \theta^n\right), \tag{18}$$

The last equation determining the evolution of the mean-field amplitude is implicit. Defining

$$y_k^n = \frac{\Delta t}{\Gamma_k}\, p_k^n\,, \qquad \kappa^n = 2(\Delta t)^2 \sqrt{J^n}\,, \tag{19}$$

the map can be rewritten with the mean-field amplitude equation explicit as the NTMF model in Eqs. (9), (3), (4), and (5) with the order parameter defined in Eq. (6). Note however that, since the change of coordinates in Eq. (19) is not canonical, the map does not preserve the area in the (θ, κ)-plane. However, this is simply an artifact of the coordinates used. By construction, according to Eq. (10), the NTMF model is symplectic in the canonical coordinates $(x_1, \dots x_N, \theta)$ and $(p_1, \dots p_N, J)$. In particular, the area in the (θ, J)-plane, as well as the area in the (x_i, p_i) planes, are preserved for $i = 1, \dots N$. The non-canonical coordinate κ is simply introduced for the convenience of expressing the evolution of the mean-field degree of freedom with an explicit map.

II.A. Period-one orbits

Introducing the $2(N+1)$-dimensional vector $\mathbf{x}^n = (x_1^n, \ldots, x_N^n, y_1^n, \ldots, y_N^n, \theta^n, \kappa^n)^\dagger$ (where $\dagger$ denotes the transpose), we write the NTMF map as

$$\mathbf{x}^{n+1} = \mathcal{M}(\mathbf{x}^n)\,, \tag{20}$$

and define a periodic orbit of order s as a sequence $\{\mathbf{x}_1^*, \ldots, \mathbf{x}_s^*\}$ such that $\mathcal{M}^s(\mathbf{x}_p^*) = \mathbf{x}_p^*$, for $p = 1, \ldots, s$. We limit attention to periodic orbits for which, for any s, the mean-field remains fixed, i.e. we assume

$$\kappa^n = \kappa^*\,, \qquad \theta^n = \theta^* = 0 \tag{21}$$

for all n, where without loss of generality we have set $\theta^* = 0$. It follows from Eqs. (4) and (5), that Eq. (21) imposes the following constraint on the order parameter and its derivative

$$\eta^n = \frac{\partial \eta^n}{\partial \theta^n} = 0\,, \tag{22}$$

for all n, evaluated at the periodic orbit.

The fixed mean-field assumption in Eq. (21) considerably simplifies the search of periodic orbits. In fact, this assumption decouples the mean-field from the particles and allows to construct the periodic orbits of the NTMF map from the periodic orbits of the standard nontwist map. In particular, from the period-one orbits analysis of the nontwist map[10], it follows that, if Eq. (22) holds, any arrangements of the N-particles such that

$$(x_k^*, y_k^*) = \left(m_k \pi,\, \pm\sqrt{1 + \frac{2\pi l_k}{a}} \right)\,, \tag{23}$$

for $k = 1, \ldots, N$, defines a period-one orbit (fixed point) of the $2(N+1)$-dimensional NTMF map, where, for each k, $m_k \in \{0, 1\}$ and $l_k \in \{0,\, 1,\, 2,\, \ldots\}$. In this case, the constraint in the order parameter η in Eq. (22) imposes the following constraint on the values of m_k and the coupling constants γ_k,

$$\sum_{k=1}^{N} (-1)^{m_k} \gamma_k = 0\,. \tag{24}$$

For example, a period-one orbit of the NTMF map can be constructed by placing half of the particles at $(x, y) = (0, 1)$ and the other half at $(x, y) = (\pi, -1)$ with $\gamma_k = 1$ for all k.

To analyze the stability of the period-one orbits we linearize the NTMF map around the fixed point $\mathbf{x}^*$. Writing, $\mathbf{x} = \mathbf{x}^* + \Delta\mathbf{x}$, we get to first order in $|\Delta\mathbf{x}|$, the linear map

$$\Delta\mathbf{x}^{n+1} = \nabla\mathcal{M}^* \Delta\mathbf{x}^n, \tag{25}$$

where $\nabla\mathcal{M}^*$ is the gradient matrix of $\mathcal{M}$ evaluated at $\mathbf{x}^*$. The stability of $\mathbf{x}^*$ is determined by the eigenvalues of $\nabla\mathcal{M}^*$, $\lambda \in \{\lambda_k\}$, with $j = 1, \ldots 2(N+1)$, which are the solutions of the characteristic polynomial

$$||\nabla\mathcal{M}^* - \lambda\mathcal{I}|| = 0 \tag{26}$$

where $\mathcal{I}$ denotes the $2(N+1) \times 2(N+1)$ identity matrix and $||\ ||$ denotes the determinant. The characteristic polynomial in Eq. (26) can be factorized as follows,

$$(1-\lambda)^2 \prod_{k=1}^{N} \mathcal{P}_k = 0, \tag{27}$$

with $\mathcal{P}_k$ given by

$$\mathcal{P}_k \;=\; \lambda^2 - 2\lambda \left[1 \pm a\kappa^* (-1)^{m_k} \sqrt{1 + 2\pi l_k / a} \right] + 1, \tag{28}$$

where the $\pm$ signs depend on the fixed point according to Eq. (23). The m-th iterate of an eigenvector $\mathbf{v}$ of $\nabla\mathcal{M}^*$, under the linearized dynamics is $[\nabla\mathcal{M}^*]^m \mathbf{v} = \lambda^m \mathbf{v}$. From here it follows that if $|\lambda| > 1$ for at least one of the eigenvalues, the fixed point is linearly unstable.

According to Eq. (27), there are two degenerate eigenvalues with $\lambda = 1$. These eigenvalues correspond to the neutral, parabolic, stability of the mean-field degrees of freedom, i.e. to perturbations of the amplitude, κ^*, and the phase, θ^*, of the mean-field. The rest of the $2N$ eigenvalues are obtained from the solution of the N quadratic equations $\mathcal{P}_k = 0$. As expected, each of these equations corresponds to the linearization of the standard nonwtwist map around the fixed point (x_k^*, y_k^*) in Eq. (23).

As an specific important example, consider a configuration with $l_k = 0$ for all k. In this case according to Eq. (23), there are four possibilities: $(x_k^*, y_k^*) = (0, 1)$, $(0, -1)$, $(\pi, 1)$, and $(\pi, -1)$. These cases correspond to the four, period-one orbits of the standard nontwist map for which it is known that $(0, 1)$ and $(\pi, -1)$ are always unstable, and $(0, -1)$ and $(\pi, 1)$ are unstable for $\kappa^* > 2/a$. From here it is concluded that a configuration of the NTMF map with all the particles located at $(0, -1)$ and $(\pi, 1)$ with the coupling constants satisfying Eq. (22) will be a stable fixed point of the self-consistent dynamics provided $\kappa^* < 2/a$.

The stability properties of the period-one orbits of the NTMF map can be used to guide the construction of self-consistent coherent states of the NTMF map. To illustrate this, we took $a = 0.8$, and a mean-field with initial conditions $\kappa^1 = 0.3064$ and $\theta^1 = 0$. For the particles we considered an ensemble of $N = 1.2 \times 10^4$ particles, with $\gamma_k = 10^{-5}$ for all k, half of them distributed in a neighborhood of the fixed point $(0, -1)$ and the other half distributed in a neighborhood the fixed point $(\pi, 1)$. For the chosen parameter values, $\kappa^1 = \kappa^* = 0.3064 < 2/a = 2.5$, which implies linear stability. Consistent with this result, Fig. 1 shows that the ensemble of particles remains coherent and the mean-field amplitude exhibits a small oscillation around κ^*.

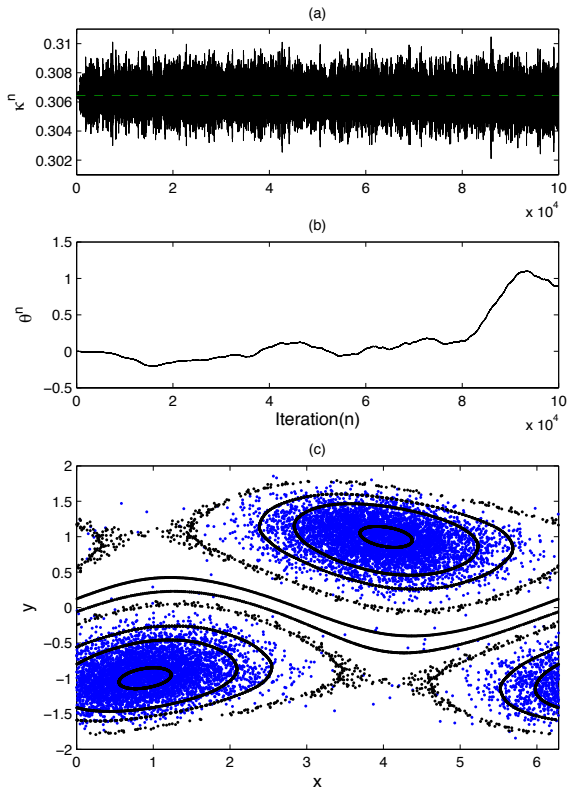

FIG. 1: Period-one coherent structure in the NTMF map. Panel (c) shows the final state in the (x_j, y_j) plane, of an ensemble of $N = 1.2\times10^4$ particles in the NTMF map with self-consistent mean-field amplitude, κ^n, and mean-field phase, θ^n, shown in panels (a) and (b) respectively. The coherence of the state is maintained by the self-consistent trapping of the particles in the period-one resonances of the nontwist map, which for each n are located at $(\theta^n, -1)$ and $(\pi + \theta^n, 1)$.

II.B. Period-two orbits

In order to find the fixed points of period-two orbits of the NTMF map we restrict attention to a fixed mean-field, i.e. $\kappa^n = \kappa^*$, $\theta^n = \theta^* = 0$, and the constraint in Eq. (22) is satisfied. Like in the period-one case, the mean-field decouples from the particles and the period-two orbits correspond to those of the standard nontwist map. In particular,

$$(x_k^*, y_k^*) = \left(m_k\pi,\, \pm\sqrt{1-\frac{\pi}{a}}\right)\,, \tag{29}$$

for $k = 1, \ldots, N$, defines a period-two orbit of the $2(N+1)$-dimensional NTMF map, where, for each k, $m_k \in \{0, 1\}$. The constraint in the order parameter, η, is the same as the one for period-one orbits in Eq. (24), and the characteristic polynomial is

$$(1-\lambda)^2 \prod_{k=1}^{N} \mathcal{Z}_k = 0, \tag{30}$$

where

$$\mathcal{Z}_k = \lambda^2 - 2\lambda\left[1 - 2a^2\kappa^{*2}(1-\pi/a)\right] + 1\,. \tag{31}$$

As before, $\lambda = 1$ is a degenerate eigenvalue corresponding to the parabolic, neutral linear stability of the mean-field amplitude and phase. Consistent with the linear stability analysis of the nontwist map, the eigenvalues obtained from the solution of $\mathcal{Z}_k = 0$ are stable provided $0 < a^2\kappa^{*2}(1-\pi/a) < 1$. That is, if this condition is satisfied, as well as the constraint in Eq. (24), then a configuration on N particles with coordinates given by Eq. (29) is a self-consistent period-two state of the NTMF map with mean-field amplitude κ^* and phase $\theta^* = 0$ Another family of period-two orbits corresponds to particles with coordinates (x_k^*, y_k^*) given by the solution of the two algebraic equations $2 - y_k^{*2} - \left(y_k^* - \kappa^* \sin x_k^*\right)^2 = 2\pi/a$ and $x_k^* = a\left(1 - y_k^{*2}\right)/2$. In this case the characteristic polynomial is not easily factorized, but numerical results and previous studies with the standard nontwist map indicate that these period-two orbits are always unstable.

Based on this linear stability analysis it is possible to construct coherent states consisting of four clusters of particles. An example is shown in Fig. 2. According to Eq. (29), the initial conditions for this calculation consisted of $N = 1.2\times10^4$ particles evenly distributed in the neighborhood of $(0, \pm\sqrt{1-\frac{\pi}{a}})$ and $(\pi, \pm\sqrt{1-\frac{\pi}{a}})$, with $a = 3.4216$. To satisfy the constraint in Eq. (24), we chose $\gamma_k = 10^{-5}$ for all k, and to guarantee the stability of the configuration, we chose the initial amplitude of the mean-field $\kappa^1 = 0.15 < 1/(a\sqrt{1-\frac{\pi}{a}}) = 1.7564$. As expected from the linear stability analysis, the mean-field amplitude and phase stay very close to their equilibrium values $\kappa^* = \kappa^1$ and $\theta^* = 0$, and the ensemble of particles remain coherent in the vicinity where they initially started.

III. SELF-CONSISTENT SEPARATRIX RECONNECTION

Separatrix reconnection is one of the main signatures of nontwist Hamiltonian dynamical systems. Because of the violation of the twist condition, resonances in nontwist systems appear in pairs, and nontrivial global bifurcations in phase space can arise due to the topologically different ways in which the unstable and stable manifolds connect. As shown in Fig. 3, in the case of symmetric nontwist maps, there are two topologically distinct phase space portraits. In the heteroclinc, or "pendulum type" topology, the unstable manifolds join the stable manifolds of adjacent hyperbolic fixed point, whereas in the homoclinic case, one of the unstable manifolds loops around the opposite elliptic fixed point and joints the stable manifold of the same hyperbolic point. These bifurcations have been studied in some detail in the literature and thresholds for the different transitions have been computed analytically and numerically. In particular, for the standard nontwist map in Eq. (8) it is known that the

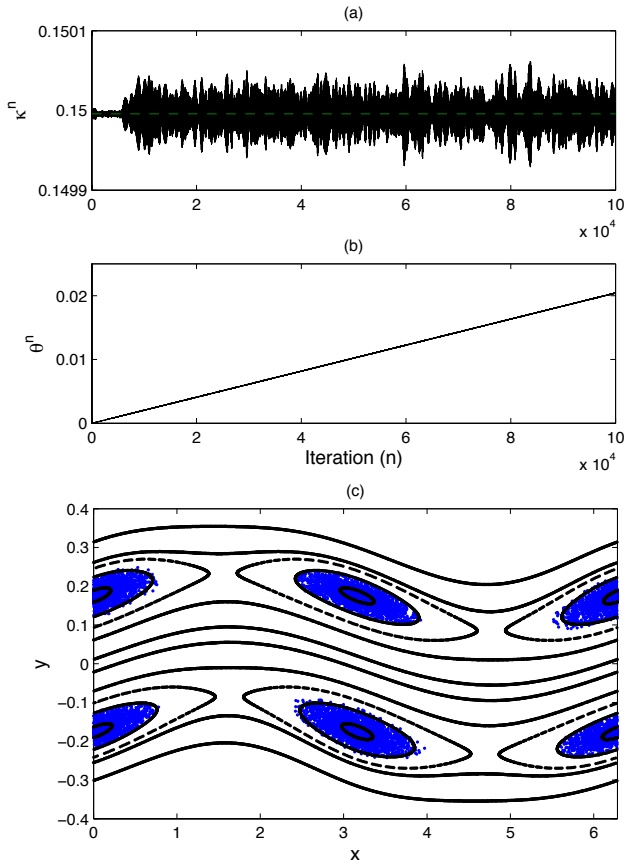

FIG. 2: Period-two coherent structure in the NTMF map. Panel (c) shows the final state in the (x_j, y_j) plane, of an ensemble of $N = 1.2\times10^4$ particles in the NTMF map with self-consistent mean-field amplitude, κ^n, and mean-field phase, θ^n, shown in panels (a) and (b) respectively. The coherence of the state is maintained by the self-consistent trapping of the particles in the period-two resonances of the nontwist map, which for each n are located at $(\theta^n, \pm\sqrt{1-\pi/a})$ and $(\theta^n+\pi, \pm\sqrt{1-\pi/a})$.

topology of period-one resonances is heteroclinic (homoclinic) when $\kappa < 2a/3$ ($\kappa > 2a/3$), with $\kappa = \kappa_{rec} = 2a/3$ denoting the reconnection threshold depicted in the middle panel of Fig. 3. This threshold follows from the analysis of the nontwist effective Hamiltonian,

$$H_{eff} = -ay + ay^3/3 + \kappa\cos(x-\theta)\,. \qquad (32)$$

As shown in Fig. 3, in the absence of chaos, the level sets of H_{eff} match the orbits of the standard nontwist map.

The global coupling in the NTMF map opens a new, unexplored phenomenology of separatrix reconnection. Contrary to the standard nontwist map, in which the topology is uniquely determined once the parameter values a and κ are fixed, in the NTMF map the evolution of the mean-field amplitude leads to dynamic separatrix reconnection, that is to bifurcations in the phase space topology as function of time. Since the mean-field amplitude depends on the state of the system, we refer to these bifurcation as self-consistent separatrix reconnection, and in this section we study its role on transport.

Despite the arbitrary large number of degrees of freedom, N, the study of separatrix reconnection in the NTMF map is relatively simple because, at any given time (iteration), the phase space topology of the j-th degree of freedom in the (x_j, y_j) phase space plane is the same for all js and it is only determined by a and the instantaneous value of κ^n. This significant simplification arises from the fact that all the degrees of freedom are subject to the same global mean-field. Based on this, we will say that the topology of the NTMF map at iteration n is heteroclinic (homoclinic) if for all $j = 1, \ldots, N$, the phase space topology in the (x_j, y_j)-plane is heteroclinic (homoclinic), that is, if $\kappa^n < 2a/3$ ($\kappa^n > 2a/3$).

The previously discussed, $\kappa_{rec} = 2a/3$, reconnection threshold arises from a simple analysis of the effective Hamiltonian in Eq. (32) corresponding to an integrable limit of the map[5]. To go beyond this estimate, and to further verify its validity, we also computed the separatrix reconnection using a more precise method based on the linear stability analysis of the period-one orbits of the map. According to this second method, the reconnection threshold at the n-th iteration, is defined as the value of a and κ^n for which the slope of the unstable eigenvector of the hyperbolic fixed point at $(\theta^n, 1)$ matches the slope of the line joining this hyperbolic point with the hyperbolic fixed point at $(\pi+\theta^n, -1)$. Note that, to be precise, we have explicitly included the dependence of the x-location of the fixed point on the phase of the mean-field, although, as mentioned before, the role of this shift is trivial in the linear stability analysis. Thus, if m_R denotes the slope of the unstable eigenvector, which according to the previously discussed linear stability analysis depends on a and κ^n, we define the reconnection threshold as the mean-field amplitude κ_{rec} for which $m_R(a, \kappa^n = \kappa_{rec}) = 2/\pi$.

To compare the two aforementioned methods for the computation of the reconnection threshold, and to study the role of self-consistent separatrix reconnection on transport, we consider a far-from equilibrium initial condition consisting of an ensemble of $N = 1.2\times10^4$ particles with $\gamma_j = 1\times10^{-5}$. At $n = 1$, the particles are uniformly distributed in two circles with radius $r_0 = 1.5$ centered around the elliptic points $(0, -1)$ and $(\pi, 1)$. We take $a = 0.055$, an initial mean-field phase, $\theta^1 = 0$, and an initial mean-field amplitude corresponding to the reconnection threshold $\kappa^1 = \kappa_{rec} = 2a/3 = 0.0367$. Figure 4 tracks the separatrix reconnection threshold conditions of the two methods as function of the iteration n. To eliminate transient effects, only data for $n \geq n_0 = 2720$ are shown. Panel (a) shows the instantaneous value of κ^n with the horizontal dashed-line denoting the κ_{rec} reconnection threshold. Points above (below) this line corresponds to mean-field amplitudes leading to homoclinic (heteroclinic) topology, while the crossings correspond to

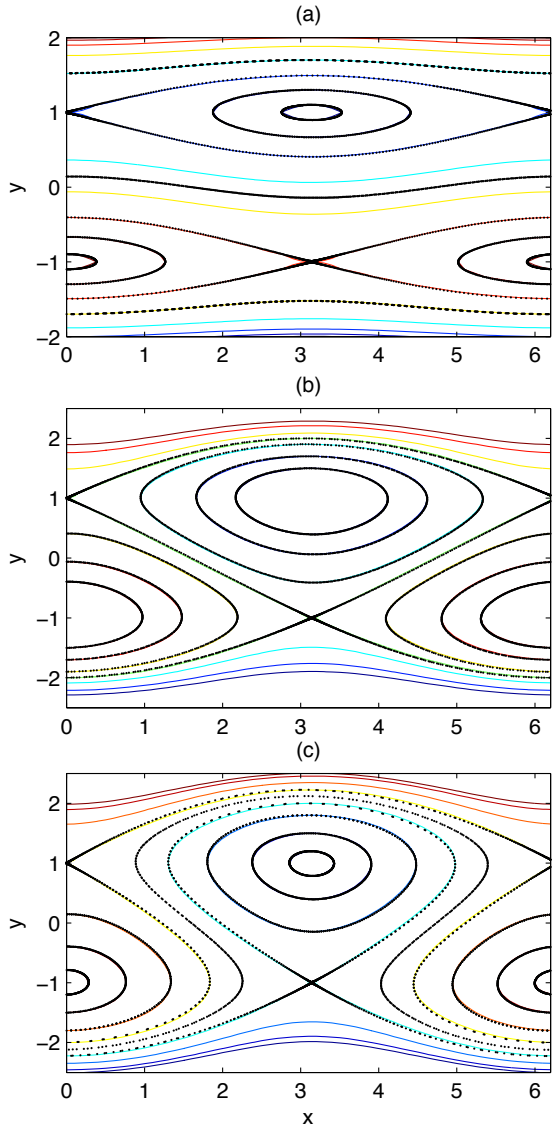

FIG. 3: Separatrix reconnection in nontwist maps. Panel (a) shows an example of the heteroclinic topology with $(a, \kappa) = (0.055, 0.00779)$; panel (c) shows and example of the homoclinic topology with $(a, \kappa) = (0.055, 0.05805)$. The reconnection threshold, corresponding to $(a, \kappa) = (a, \kappa_{rec} = 2a/3) = (0.055, 0.0367)$, is shown in panel (b). The dotted lines correspond to the map iterations and the solid lines to the level sets of H_{eff} in Eq. (32). As shown in Fig. 4, in the NTMF map, self-consistent separatrix reconnection gives rise to a dynamic, time-dependent transition between the two topologies.

reconnection states. The curve in panel (b) of Figure 4 shows the absolute value of the slope of the eigenvector of the unstable fixed point as function of n. The horizontal, dashed line denotes the slope, $m_R = 2/\pi = 0.636$, of the line joining the two hyperbolic points. According to the eigenvector criterion, the intersections of the curve with the horizontal line correspond to the reconnection states. Comparison of panels (a) and (b) of Fig. 4, indicates that there is a very good agreement between the two methods. This result is particularly valuable since it provides further support to the simple reconnection threshold estimate $\kappa_{rec} = 2a/3$.

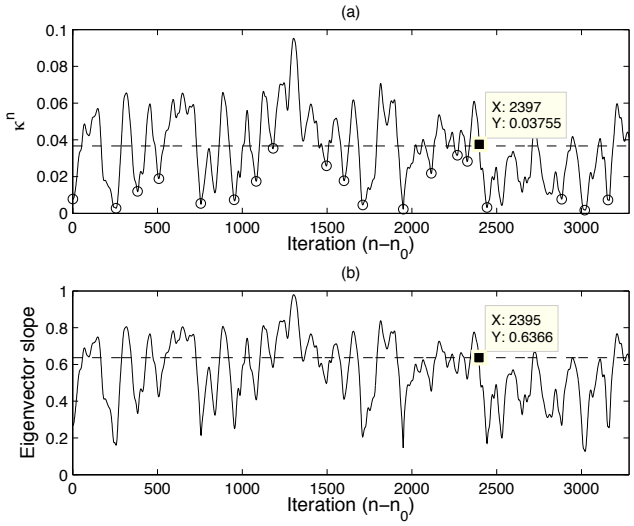

FIG. 4: Dynamic, self-consistent separatrix reconnection in the NTMF map. Panel (a) shows the instantaneous values of the mean-field amplitude, κ^n. The horizontal dashed line, corresponds to the reconnection threshold $\kappa_{rec} = 2a/3 = 0.0367$. Values above (below) this line correspond to the homoclinic (heteroclinc) topology. Panel (b) shows the instantaneous value of the slope of the eigenvector of the unstable fixed point as function of n. In agreement with the criterion shown in (a), the reconnection states are given by the intersections with the $m_R = 2/\pi = 0.636$ horizontal dashed line. The circles denote specific values of n used in the study of transport in Figs. 5 and 6.

To conclude this section, we discuss the role of self-consistent separatrix reconnection on transport. As it is well known, in the standard nontwist map, transport across the shearless curve can only take place for parameter values for which the shearless curve has been destroyed due to chaos. However, in the NTMF map, self-consistent dynamic reconnection can give rise to transport across the sheareless curve even in the case when the values of κ^n never reach the threshold for the destruction of the shearless curve. Figure 5 shows evidence of this novel, self-consistent, reconnection-driven transport mechanism. The different panels in this figure track the evolution of a concentrated patch of $5,000$ *passive particles* in the (x, y)-plane evolving under the NTMF map used in the study of reconnection in Fig. 4. In this calculation it is important to distinguish between active and passive particles. The active particles are the ones used to create the mean-field. In this case, they correspond to the ensemble of particles uniformly distributed in two circles with radius $r_0 = 1.5$ centered around the

elliptic points $(0,-1)$ and $(\pi,1)$. As discussed before, the self-consistent interaction of these particles gives rise to the variations of the mean-field amplitude sown in Fig. 4-(a). On the other hand, the *passive particles* depicted in Fig. 5, simply follow the evolution in the (x,y) plane of a standard nontwist map of the form in Eq. (8) for which, at each iteration n, the value of κ and θ is given by the instantaneous values of κ^n and θ^n of the NTMF map shown in Fig. 4-(a).

In addition to the distribution of the passive particles, Fig. 5 also shows the instantaneous location of the shearless curve and the separatrices of the period-one resonances. The separatrices were obtained from the level sets of the effective Hamiltonian, H_{eff}, in Eq. (32). Tracking the location of the shearless curve is a harder problem which can be approached using two complementary techniques: periodic orbits approximations[10] or indicator points[13]. Here we use indicator points as they provide a relatively straightforward way to locate the shearless curve for any rotation number. An indicator point is a point that is guaranteed to belong to the shearless curve when this curve exists. For the standard nontwist map an indicator point is given by

$$\mathbf{x}_{ind} \;=\; (\pi/2+\theta^n, \kappa^n/2)\,. \tag{33}$$

What this means in terms of the computations is that, if for a given n, the shearless curve exists, it can be obtained for given values of (a,κ^n,θ^n) by iterating the standard nontwist map for the initial condition in Eq. (33). It is critical to point out that the level of chaotic transport in Fig. 5 is negligible, as the value of κ^n stays very small throughout the self-consistent evolution. In particular, κ^n, stays way below the threshold for the destruction of the shearless curve. Nevertheless, as shown in the Fig. 5, there is transport across the central barrier. This non-chaotic transport is driven by the changes in the phase space topology caused by self-consistent separatrix reconnection.

To quantify the transport across the CTB we consider the ratio, Λ, of the number of particles above the shearless curve to the total number of particles. In doing this calculation we used the indicator points of the nontwist map to track the location of the shearless curve at each iteration n. Figure 6 shows Λ as function of n, where, as in the study of reconnection, we have eliminated the transient effects. As the first panels in Fig.5 show, initially, separatrix reconnection transports the whole distribution of particles across the CTB, and the value of Λ drops to zero. At later times, the combined effects of separatrix reconnection and (non-chaotic) mixing at hyperbolic fixed points homogenizes the distribution of particles across the central barrier, and Λ reaches the asymptotic state $\Lambda = 1/2$.

IV. SELF-CONSISTENT CHAOTIC TRANSPORT

In addition to the trivial, fully integrable regime, in which all invariant circles exists, one can distinguish two non-integrable regimes in nontwist systems: banded chaos and global chaos[5]. The banded chaos regime is characterized by the existence of robust CTBs flanked by bands of chaotic regions. On the other hand, global chaos is characterized by the destruction of all the CTBs and the existence of widespread chaotic transport. In the case of the standard nontwist map these regimes, which are uniquely determined by the values of a and κ, have been studied in considerable detail in the literature. However, as in the case of separatrix reconnection, the self-consistent coupling in the NTMF map brings novel dynamic phenomena.

Once again, the mean-field nature of the coupling simplifies the analytical and numerical study for an arbitrary number of degrees-of-freedom. In particular, since all the degrees of freedom behave in the same way, we will say that the NTMF model exhibits banded (global) chaos at iteration n, if the corresponding standard nontwist map in the (x_k,y_k) plane with $\kappa=\kappa^n$ exhibits banded (global) chaos. However, the key novel issue is that, because of the self-consistent coupling, in the NTMF model the mean-field amplitude evolves with n and therefore a nontrivial transition among different transport regimes can take place. In this section we focus on the study of the following three transport scenarios that exhibit transitions among the aforementioned regimes due to the self-consistent evolution of the mean-field amplitude: (i) Self-consistent suppression of diffusion; (ii) Self-consistent CTB destruction; and (iii) Intermittent transport near criticality.

IV.A. Suppression of diffusion

As a case study of a self-consistent transition from a state at the threshold of global chaos, to banded chaos, and eventual full integrability, we consider a problem in which $\kappa^n \to 0$ as $n\to\infty$, with κ^1 corresponding to the onset of global chaos. In this case, the diffusive transport expected to be present in the chaotic regime is suppressed as KAM surfaces reform while the system approaches full integrability.

We consider an initial condition consisting of $N = 6\times 10^3$ particles with $\gamma_k = 10^{-6}$, and $N = 6\times 10^3$ particles with $\gamma_k = -10^{-6}$. The $\gamma_k>0$ ($\gamma_k<0$) particles are uniformly distributed along the x-direction and have a Gaussian distribution along the y-direction with standard deviation equal to 0.25 and mean $\overline{y_k}=10$ ($\overline{y_k}=-10$). Since we are interested on initial states at the threshold of global chaos, we took $a=a_\gamma$, $\kappa^1=\kappa_\gamma$, and $\theta^1=0$, where $(a_\gamma,\kappa_\gamma) = (4.31062700354, 0.742493131039)$ are the threshold values for the onset of global chaos when the rotation number of the shearless curve is the in-

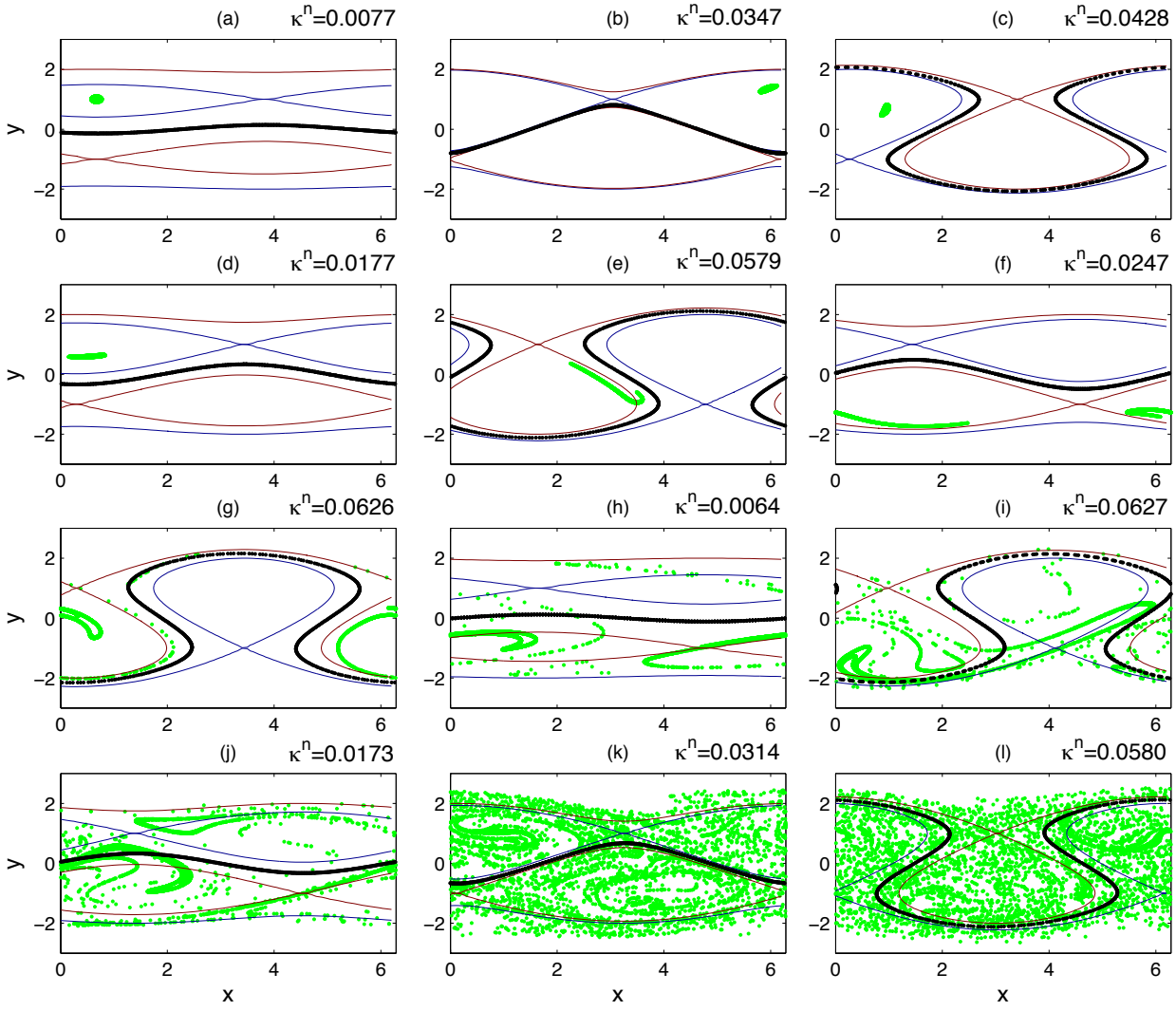

FIG. 5: Nonchaotic global transport driven by dynamic separatrix reconnection. The successive panels follow the evolution of an initially localized ensemble of passive tracers, for $n - n_0 = 1, 50, 110, 194, 450, 498, 658, 760, 880, 940, 1480$ and 1664. The dynamic, self-consistent separatrix reconnection shown in Fig. 4, along with the nonchaotic mixing near the hyperbolic fixed points, homogenizes the tracer across the shearless central transport barrier (dark bold curve). For reference, the instantaneous separatrices corresponding to the level sets of the effective Hamiltonian, H_{eff}, in Eq. (32) with $\kappa = \kappa^n$, and $\theta = \theta^n$, are also shown.

verse golden mean, $1/\gamma$. Note that, to simplify the notation, Eq.(9) corresponds to the standard nontwist map in Ref. 10 with the x-coordinated rescaled as $x \to x/(2\pi)$. Accordingly, the threshold value that we use is the one reported in Ref. 10, $a = 0.686049\ldots$, multiplied by 2π.

The self-consistent suppression of diffusion in the NTMF model for these initial conditions and parameter values is evident in the time evolution of the ensemble averaged, second moment of the $\gamma_k > 0$ particles' displacements,

$$\langle (\Delta y)^2 \rangle (n) = \frac{1}{N} \sum_{k=1}^{N} (y_k^n - y_k^1)^2 \,. \tag{34}$$

In particular, as shown in Fig. 7, $\langle (\Delta y)^2 \rangle (n)$, exhibits an initial growth followed by an exponential saturation at large n, resulting from transport suppression.

The corresponding self-consistent decay of the mean-field amplitude, κ^n, is shown in a logarithmic scale in panel (a) of Fig. 8, along with the evolution of the phase of the mean-field, θ^n in panel (b). The evolution of the particles' density function (pdf) in y, averaged over x, is

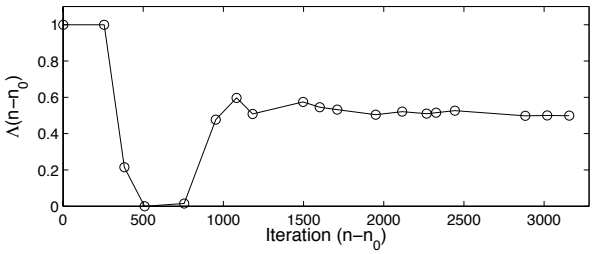

FIG. 6: Ratio of particles, Λ, transported across the shearless, central transport barrier due to dynamic separatrix reconnection. Consistent with Fig. 5, the initial condition of tracers located above the shearless, is eventually homogenized at both sides of the barrier. The offset n_0 is used to eliminate the transients in the NTMF map.

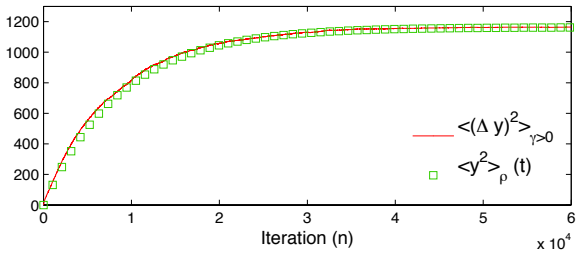

FIG. 7: Second moment of particles' displacements during self-consistent suppression of diffusion in the NTMF map. The solid line denotes the ensemble average second moment in Eq. (34). The squares denote the second moment of the pdf, ρ, of the $\gamma > 0$ particles in the effective quasilinear transport model according to Eq. (41).

shown in Fig. 9. Only the pdf for the $\gamma_k > 0$ particles, $\rho_{\gamma>0}$, is shown. By symmetry, the distribution function for the $\gamma_k < 0$ particles is $\rho_{\gamma<0}(y,t) = \rho_{\gamma>0}(-y,t)$. In agreement with the fact that κ^n drops below the critical value for global chaos, the pdf exhibits a transport barrier around $y = 0$. Also, consistent with the asymptotic saturation at large n of the second moment, the distribution, $\rho_{\gamma>0}$, exhibits a relaxation towards the steady state shown in Fig. 9-(d)

Quasilinear theory, when it works, provides a simple, appealing description of transport in chaotic systems. In particular, in the case of area-preserving maps of the form in Eq. (1), the quasilinear diffusivity, $D_{QL} = (1/4\pi)\int_0^{2\pi} f^2(x)dx$, yields a low order, approximate model describing diffusive transport in y. In the case of mean-field models, a direct application of the quasilinear prescription to Eq. (3) gives the self-consistent diffusivity

$$D^n_{QL} = \frac{(\kappa^n)^2}{4}\,. \tag{35}$$

Although there is no a priori reason for its justification, as we will show below, this time dependent quasilinear diffusion provides a good model to describe suppression of diffusion in the NTMF map. As a first step to show this, note that, according to Fig. 8-(a), the dynamics of κ^n is well fitted by an exponential decay of the form $\kappa^n = \kappa_0 e^{-n\nu}$, which according to Eq. (35) implies $D^n_{QL} = \frac{\kappa_0^2}{4}e^{-2n\nu}$.

Motivated by this, we propose the diffusion equation with time-dependent diffusion coefficient

$$\frac{\partial\rho}{\partial t} = D_{QL}(t)\,\frac{\partial^2\rho}{\partial y^2}\,, \tag{36}$$

as an effective transport model describing the spatio-temporal evolution of the particles' pdf, ρ, where, for simplicity, we have dropped the "$\gamma > 0$" sub-index, and the time dependent diffusivity,

$$D_{QL}(t) = \frac{\kappa_0^2}{4}e^{-2t\nu}\,, \tag{37}$$

corresponds to the continuous-in-time limit of the discrete quasilinear diffusivity D^n_{QL}.

To test the validity of the quasilinear model to describe transport suppression in the NTMF model we solve Eqs. (36) and (37) in the semi-infinite interval, $y \in (0,\infty)$. Because the CTB forms relatively fast and remains there for all $t > 0$, the particle flux through it is zero. Accordingly, although the CTB is not exactly localized $y = 0$, we impose the zero-flux, Neumann boundary condition:

$$\left.\frac{\partial\rho}{\partial y}\right|_{y=0} = 0\,. \tag{38}$$

To solve Eq. (36), we first perform the invertible change of variables,

$$\tau(t) = \int_0^t D_{QL}(t')dt' = \frac{\kappa_0^2}{8\nu}\left[1 - e^{-2\nu t}\right]\,, \tag{39}$$

and transform Eq. (36) into the simple, time-independent diffusion equation

$$\frac{\partial\rho}{\partial\tau} = \frac{\partial^2\rho}{\partial y^2}\,. \tag{40}$$

The very good agreement shown in Fig. 9, between the NTMF model and the well-known solution of the diffusion equation in Eq. (40) with $\tau = \tau(t)$ given by Eq. (39), gives support to the validity of the quasilinear model.

From Eqs. (40) and (39) it follows that the time evolution of the second moment, $\langle y^2\rangle_\rho = \int_0^\infty y^2\rho dy$, is

$$\langle y^2\rangle_\rho(t) = 2\tau(t) = 2\frac{\kappa_0^2}{8\nu}\left[1 - e^{-2\nu t}\right]\,. \tag{41}$$

Figure 7 compares Eq. (41) with the time evolution of the second moment in Eq. (34) obtained from the ensemble average of the NTMF model.

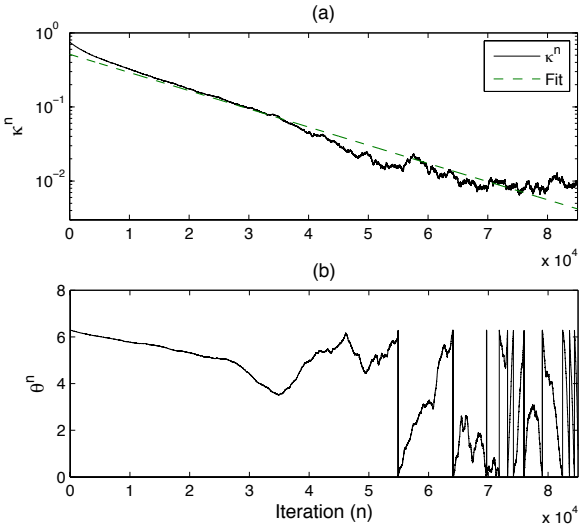

FIG. 8: Mean-field evolution during self-consistent suppression of diffusion in the NTMF map. Panel (a) shows the decay of κ^n, in log-normal scale. The dashed line corresponds to the exponential fit $\kappa^n = \kappa_0\, e^{-n\nu}$ with $\kappa_0 = 0.5162$ and $\nu = -5.7274 \times 10^{-5}$. Panel (b) shows the evolution of the phase θ^n which, in support to the random-phase approximation, exhibits stochastic fluctuations at intermediate and large times.

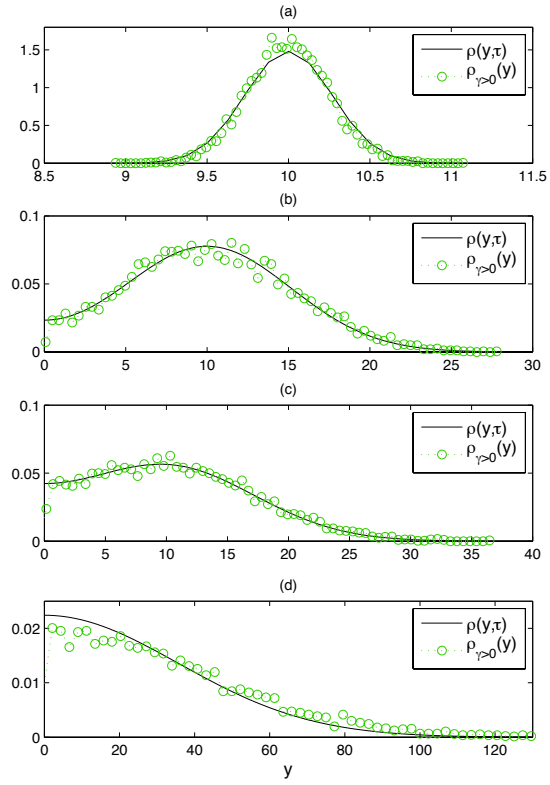

FIG. 9: Spatio-temporal evolution of probability density function of $\gamma > 0$ particles during self-consistent suppression of diffusion. The circles denote the pdfs obtained from the histograms of an ensemble of particles evolving under the NTMF map. The solid lines denote the analytical solution of the effective time-dependent diffusion model in Eqs. (36) and (37). Panels (a), (b), (c) and (d) correspond to $n = 1$, 100, 200 and 49900 respectively.

As an additional test of quasilinear diffusion, we considered the same initial conditions used in the study of suppression of diffusion above, but for different initial values of the mean-field amplitude, κ^1. For each κ^1, we iterated the NTMF map $\mathcal{T}$-times, and computed the time-averaged mean-field amplitude, $\overline{\kappa}$, and diffusivity, $\overline{D}$,

$$\overline{\kappa} \;=\; \frac{1}{\mathcal{T}}\sum_{n=1}^{\mathcal{T}} \kappa^n\,, \qquad \overline{D} = \frac{1}{\mathcal{T}}\sum_{n=1}^{\mathcal{T}} D^n\,. \tag{42}$$

For each n, the instantaneous diffusivity, D^n, was calculated from the statistics of the displacements of an ensemble of 1×10^4 *passive particles* iterated 1.5×10^4 times with the standard nontwist map with $\kappa = \kappa^n$ and $\theta = \theta^n$. For each κ^1, the value of $\mathcal{T}$ was chosen large enough to guarantee convergence to steady state. These values ranged from $\mathcal{T} = 2 \times 10^4$ for $\kappa^1 = 0.2$, to $\mathcal{T} = 1.1 \times 10^5$ for $\kappa^1 = 0.87$. The large values of $\mathcal{T}$, required the computation of a large number of instantaneous diffusivities, D^n, each of which required by itself the iteration of the standard nontwist map for a large number of iterations for many initial conditions. To perform this calculation in a reasonable time, we used Graphics Processing Units (GPUs) which are a powerful computational resource that can be used to accelerate particle based computations. The results of the computation are shown in Fig. 10 where the circles, with increasing values of $\overline{\kappa}$, correspond to $\kappa^1 = \{0.2, 0.5, 0.8, 0.87, 0.95, 1, 1.1, 1, 3, 1.5\}$, and the solid line corresponds to the time-averaged quasilinear diffusivity prediction, $\overline{D}_{QL} = \overline{\kappa}^4/4$.

IV.B. Transition to global chaos

In this section we study transport in the case when the self-consistent mean-field coupling takes the system from a banded-chaos state, in which there is a robust CTB, to a state of global chaos in which the CTB has been destroyed.

The initial condition consists of an ensemble of $N = 1.2\times10^4$ particles with $\gamma_k = 10^{-6}$, uniformly distributed along the x-axis, and as a Gaussian distribution along the y-axis with mean, $\overline{y} = -150$, and standard deviation equal to 0.5. For the map parameter a, we took the critical value for the destruction of the $1/\gamma$ shearless curve, $a = a_\gamma = 4.31062700354$. For the initial phase of the mean-field and the initial amplitude we took $\theta^1 = 0$ and $\kappa^1 = 0.7$, which is a value slightly below the critical amplitude, $\kappa_\gamma = 0.74249$, for the destruction of $1/\gamma$ shearless CTB.

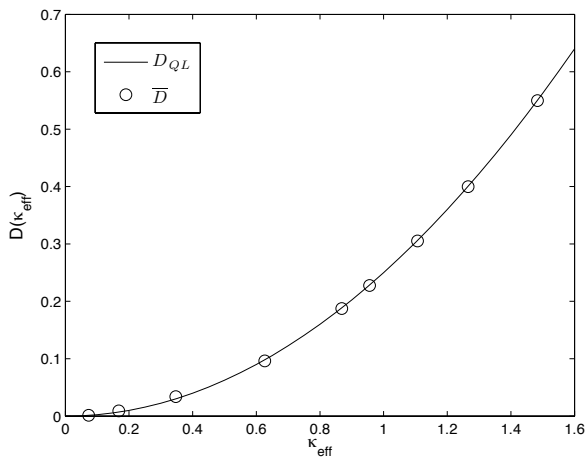

FIG. 10: Time averaged diffusivity, $\overline{D}$, as function of time averaged mean-field amplitude, $\overline{\kappa}$, in Eq. (42). The circles denote the numerical results obtained from the NTMF map for different mean-field initial conditions κ^1. The solid line corresponds to the quasilinear relation $\overline{D} = \overline{\kappa}^2/4$.

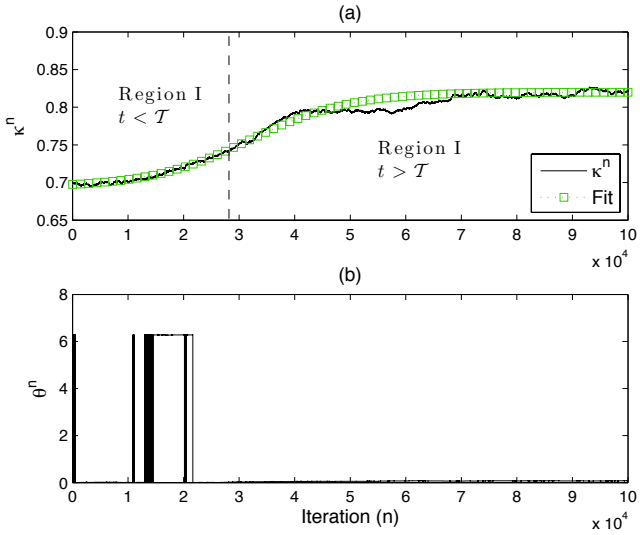

FIG. 11: Mean-field evolution during self-consistent transition to global chaos in the NTMF map. The solid line in panel (a) shows the growth and saturation of κ^n. The squares corresponds to the fit, $\kappa^n = K + \alpha \tanh\left(\frac{n-\mu}{\beta}\right)$, with $K = 0.757$, $\alpha = 0.063$, $\mu = 3.2 \times 10^4$ and $\beta = 1.8 \times 10^4$. The vertical dashed line denotes the transition to global chaos due to the destruction of the shearless, central transport barrier. Panel (b) shows the evolution of the phase θ^n which, for the most part, stays at $\theta^n = 0$.

The self-consistent transition to global chaos is observed in Fig. 11 that shows the evolution of mean-field amplitude, κ^n, and phase, θ^n. In particular, as indicated by the vertical dashed line, around $n = 28,800$, κ^n crosses the threshold for the destruction of the shearless CTB. As Fig. 14 shows, this transition manifests as a change in the linear growth rate of the second moment of the particles' displacements.

Following the procedure of the previous sub-section, we use a quasilinear description to model transport. In this case, as Fig. 11 shows, the evolution of the mean-field amplitude is well-fitted by the function, $\kappa^n = K + \alpha \tanh\left(\frac{n-\mu}{\beta}\right)$, with $K = 0.757$, $\alpha = 0.063$, $\mu = 3.2 \times 10^4$ and $\beta = 1.8 \times 10^4$. For this $\kappa(n)$, the quasilinear prescription in Eq. (35), leads to the time-dependent diffusivity,

$$D_{QL}(t) = \frac{1}{4}\left[K + \alpha \tanh\left(\frac{t-\mu}{\beta}\right)\right]^2 . \qquad (43)$$

As before, the change of variables, $\tau(t) = \int_{t_0}^{t} D_{QL}(t')dt'$, reduces the problem to the solution of the diffusion equation in Eq. (40).

To account for the dynamic destruction of the CTB, we divide the solution of the diffusion equation in two parts. As mentioned above, when $0 \leq t \leq \mathcal{T}$, where $\mathcal{T} \approx 2.88 \times 10^4$, there is a robust CTB. Therefore, in this time interval, the diffusion equation is solved in the semi-infinite domain $y \in (-\infty, 0)$ with the zero-flux, Neumann boundary condition in Eq. (38). Outside this interval, i.e., for $t > \mathcal{T}$, there is global chaos and the diffusion equation is solved in the $y \in (-\infty, \infty)$ domain. The matching of the two solutions is done by using the solution of the first problem at $t = \mathcal{T}$, as the initial condition of the second problem. Figures 12 and 13 show an excellent agreement between the numerical results obtained with the NTMF model and the solutions of the first and the second problems respectively. A further test of the quasilinear diffusion model is provided by the comparison of the rate of change of the second statistical moment in the Fig. 14. The diffusive model reproduces well the transition in the rate of change of the growth of the second moment. There is however an offset in the transition point. This is likely related to the fact that, as we will discuss in the next subsection, near the transition, the fluctuations of κ^n around the critical value, κ_γ, give rise to an intermittent destruction and formation of the CTB. This intermittency creates a "semi-impermeable" barrier at $y = 0$ not captured by the simple diffusion model.

IV.C. Intermittent transport near criticality

In the study of the self-consistent transition to chaos presented in the previous section, it was observed that near the critical point, i.e. for values on n for which $\kappa^n \approx \kappa_\gamma$, transport across the CTB slightly deviates from the predictions of the quasilinear diffusion model. In particular, as a consequence of the intermittent destruction and reappearance of the shearless curve, the region around $y = 0$ acts as a nondiffusive leaky barrier which manifests as an offset in the transition of the rate

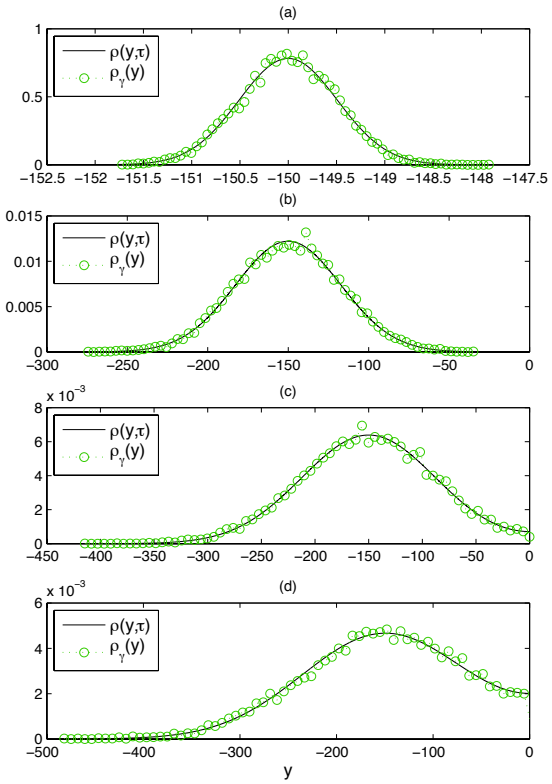

FIG. 12: Spatio-temporal evolution of probability density function before the onset of global chaos marked by the vertical dashed line in Fig. 11. The circles denote the pdfs obtained from the histograms of an ensemble of particles evolving according to the NTMF map. The solid lines denote the analytical solution of the effective time-dependent diffusion model in Eqs. (36) and (43), with boundary condition in Eq. (38). Panels (a), (b), (c) and (d) correspond to $n = 1$, 4380, 15780 and 28800 respectively. The late time evolution, after the onset of chaos, is shown in Fig. 13.

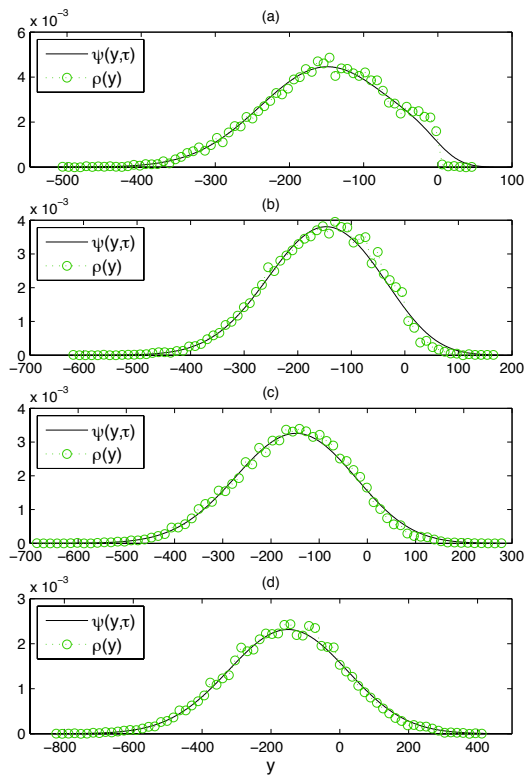

FIG. 13: Same as Fig. 12, but for late time evolution after the onset to global chaos where the diffusion model is solved in the domain $(-\infty, \infty)$. Panels (a), (b), (c) and (d) correspond to $n = 31380$, 42200, 55300 and 99780 respectively.

of change of the second moment in Fig. 14. To study in more detail this near criticality transport regime we consider the NTMF map with the same initial conditions used in the transition to global chaos of the last section.

For each value of κ^n in the interval $n \in (1, 3 \times 10^4)$ we determined the existence of the shearless curve using the indicator point method (as explained following Eq. (33) proposed and tested in Ref. 13. To implement the method in the case of the NTMF map, for a given value of κ^n and θ^n, we iterated the standard nontwist map in Eq.(8) M times with $\kappa = \kappa^n$ and $\theta = \theta^n$ and initial condition $(x_0, y_0) = (\pi/2 + \theta, \kappa)$. If, for this initial condition, there is a j such that $|y_j| > \pi$, then it was concluded that the shearless curve in the NTMF map did not exist. The rationale behind this criterion is that, for the standard nontwist map, the shearless curve, when it exists, is bounded in the $y \in (\pi, \pi)$ interval, and it can be generated from the initial condition $(x_0, y_0) = (\pi/2+\theta, \kappa)$ known as the indicator point. In principle, M should be

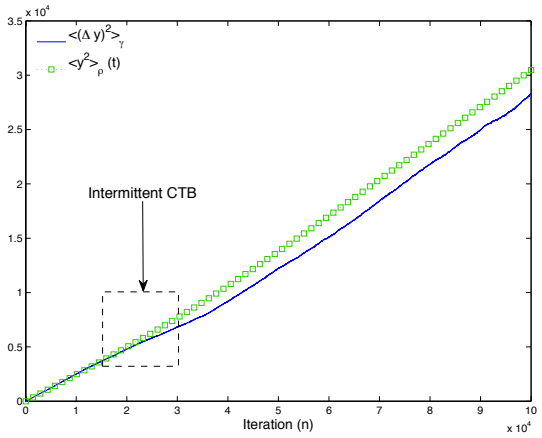

FIG. 14: Second moment of particles' displacements during self-consistent transition to global chaos in the NTMF map. The solid line denotes the ensemble averaged second moment in Eq. (34). The squares denote the second moment of the pdf, ρ, in the effective quasilinear transport model. The rectangle in dashed lines shows the transition to global chaos due to the destruction of the central transport barrier.

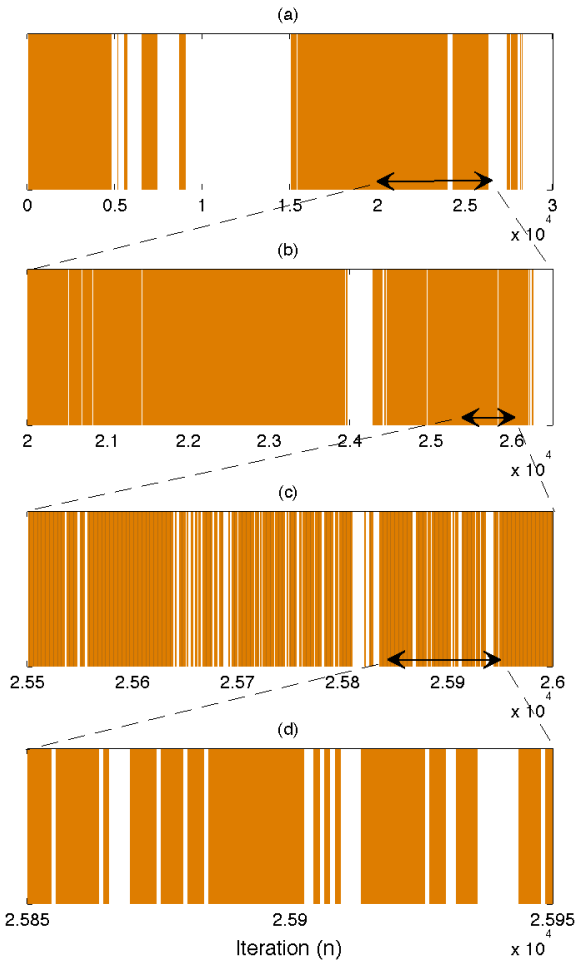

FIG. 15: Fractal binary plot showing the dynamic transition to global chaos in the NTMF map near criticality. The dark (white) stripes denote time intervals where the shearless, central transport barrier exists (does not exist). The successive zooms shown in panels (b) and (c) reveal a Cantor-like set structure corresponding to a fat fractal with scaling exponent $\beta = 0.6597$ (see Fig. 16).

an arbitrarily large number. However, in actual computations M is a finite, large number. In the calculations reported in this paper we used $M = 2 \times 10^5$. Convergence was tested by observing that the results remained unchanged for $M > 2 \times 10^5$. The result of this calculation is shown in the binary plot in Fig.15-(a) where the bars (white spaces) denote ranges in which the shearless curve exists (is destroyed). The self-similar structure of the plot is evident from the successive zooms shown in panels (b), (c) and (d). An apparent solid stripe at one scale exhibits a highly nontrivial pattern of intertwined solid and white stripes at finer scales, reminiscent of a Cantor set. However, although the set of dark stripes in Fig. 15 exhibits self-similarity, its fractal dimension calculated using the box counting method equals one. In this sense, this set resembles more a fat Cantor set than a regular Cantor set. A regular Cantor set is obtained by successively deleting the central 1/3 of each segment, and as it is well known, its fractal dimension is $\log 2/\log 3$. On the other hand, the set obtained by deleting the central 1/3 at the first iteration, then the central 1/9, then the central 1/27 and so on, is a fat Cantor set whose fractal dimension is one[14].

Like in the case of fat Cantor sets, the fractal dimension, being an integer, does not characterize the self-similar scaling properties seen in Fig. 15. As an alternative, we consider the characterization of fat fractals proposed in Ref. 15. For a given scale of resolution, ϵ, we consider the coarse-grained measure,

$$\mu(\epsilon) = 1 - h(\epsilon)\,, \tag{44}$$

where $h(\epsilon)$ is the total size of the stripes in Fig. 15 whose width is greater than, or equal to, ϵ. Figure 16 shows a plot of $\Delta\mu = \mu(\epsilon) - \mu(0)$ as function of ϵ. For consistency with Eq. (44), in the calculation the time was rescaled to map the interval in Fig. 15-(a) to the unit interval $[0, 1]$. In agreement with the conjecture put forward in Ref. 15, there is algebraic scaling of the form

$$\mu(\epsilon) = \mu(0) + A\epsilon^{\beta}\,, \tag{45}$$

with $A \sim 1$, $\mu(0) = 0.2872$, and $\beta = 0.6597$.

The exponent β, known as the *fatness exponent*, is the key parameter to characterize the self-similar properties of the set. For non-fractal objects this number diverges, $\beta \to \infty$, and for regular fractals it is trivially related to the fractal dimension d, according to $\beta = D - d$ where D is the Euclidean dimension of the embedding space. However, for fat fractals β is independent of d and it describes the scaling of the size of the gaps with the resolution[15].

V. SUMMARY AND CONCLUSIONS

In this work we have a studied the role of mean-field coupling in area-preserving nontwist maps. Nontwist Hamiltonian systems in general, and nontwist maps in particular, have recently received considerable attention in the mathematical and applied dynamical systems communities. The violation of the twist condition has motivated the generalization of previous mathematical results, including, among others, the KAM theorem and Green's residues criterion, to this type of systems. From an applied perspective, nontwist Hamiltonian systems have been used to describe chaotic transport in fluids and plasmas, stochastic magnetic fields in controlled nuclear fusion devices, particle accelerators, ray propagation in waveguides, superconducting quantum interference devices, and atomic physics, among others. However, these previous studies have restricted attention to low-degrees-of freedom systems.

As a first step to go beyond the relatively well-understood two-dimensional area-preserving nontwist maps, we proposed and studied an N-dimensional, nontwist mean-field (NTMF) model. In this model, the N

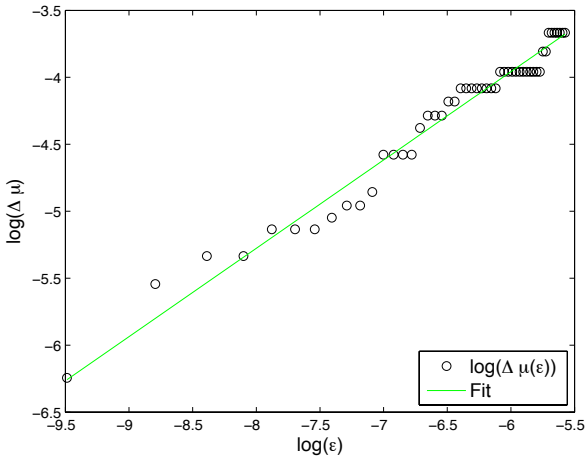

FIG. 16: Power law scaling of gaps' size with resolution scale during intermittent transport near criticality in the NTMF map. The circles denote the data from the binary plot in Fig. (15). The solid line denotes a fit to the algebraic decay in Eq. (45) with $A \sim 1$, $\mu(0) = 0.2872$, $\beta = 0.6597$.

degrees of freedom of the system interact through a self-consistently mean-field. The type of the mean-field coupling is motivated by the coupling used in the Single Wave Model (SWM) which is a Hamiltonian mean-field model that describes the weakly nonlinear dynamics of marginally stable plasmas and fluids. A natural place to look for potential applications of the nontwist mean-field model is in reduced, weakly nonlinear descriptions of fluids and plasmas. As discussed in Ref.[1], the twist mean-field model provides a reduced description of vortex dynamics in the presence of a strong monotonic background shear flow. This motivates the exploration of applications of nontwist mean-field models to problems in which the background shear flow is not monotonic. In this regard, the work on Ref.[16] (where analogues of the Single Wave Model were derived for non-monotonic shear flows) would provide a valuable first step.

A problem of considerable interest in systems with many degrees-of-freedom systems is the formation of coherent structures. Based on the linear stability properties of period-one and period-two orbits, we showed the existence of coherent states in the NTMF model. The coherence of these states is maintained by the self-consistent trapping of the particles in the resonances of the mean-field.

One of the main signatures of nontwist systems is separatrix reconnection, which is a global bifurcation resulting from the topologically different ways in which the stable and unstable manifolds of fixed points link. In the NTMF model the mean-field coupling gives rise to self-consistent separatrix reconnection. We have shown that the dynamic evolution of the phase space topology caused by self-consistent separatrix reconnection can lead to transport across the central, shearless transport barrier even in the absence of chaos. It is important to mention that this novel transport mechanism is fundamentally different from the chaotic transport that arises due to the break-up of KAM curves. In the numerical results shown, the mean-field amplitude stays relatively small during the self-consistent separatrix reconnection. In particular, for each, n, the corresponding standard nontwist map with $\kappa = \kappa^n$ has a negligible amount of chaos.

In the study of self-consistent chaotic transport we considered three problems: (i) Suppression of diffusion; (ii) Self-consistent destruction of the CTB; and (iii) Intermittent transport near criticality. In the first problem the self-consistent coupling leads to the decay of the mean-field amplitude. This decay results in a decrease of transport due to the formation of transport barriers. In particular, it was observed that, for large n, the growth of the second moment saturates and the particle distribution function reaches a steady state. In the study of the second problem, we consider a transport regime in which the coupling leads to a self-consistent growth of the mean-field amplitude. This growth results in a transition from a state of banded chaos, with a robust CTB, to a state of global chaos, in which the CTB has been destroyed. For both problems, suppression of diffusion and self-consistent destruction of the CTB, we constructed time-dependent quasilinear diffusion transport models describing the spatio-temporal evolution of the particles' probability density function. It is interesting to point out that, in the study of suppression of diffusion, quasilinear theory gives good results even when the mean-field amplitude, κ^n, is small. A further test of quasilinear theory was presented by comparing the time-averaged diffusion coefficient with the time-average mean-field amplitude, for a family of numerical solutions of the NTMF map. At first hand, the agreement with quasilinear diffusion seems puzzling, since the random phase approximation is expected to be valid in the highly non-integrable chaotic regime. However, in the case of the NTMF map, a key issue is that the decay of κ^n is accompanied by an apparent stochastic evolution of the phase of the mean-field, θ^n, which leads support to the random-phase approximation assumed in quasilinear theory. A similar situation was observed in the study of coupled twist maps in Ref. 2.

It is well-known that the transition to chaos due to the breakup of KAM curves in area-preserving maps exhibits self-similar scaling behavior in the vicinity of the critical transition point. To explore the role of mean-field coupling in this scaling behavior, we studied the self-consistent dynamics of the NTMF map near the critical point. It was observed that the self-consistent fluctuations of the mean-field amplitude around the critical point give rise to the intermittent destruction and formation of the shearless central transport barrier. The binary plot of the existence and destruction of the shearless curve, exhibits a Cantor-set-like self-similar structure. However, as in the case of fat Cantor sets, the frac-

tal (box counting) dimension, being an integer in this case, does not characterize the self-similarity of the set. As an alternative, we used the characterization of fat-fractals based on the scaling properties of the size of the gaps with the resolution scale. Self-similar, algebraic decay was observed with a fatness exponent, $\beta = 0.6597$.

ACKNOWLEDGEMENTS

LC and JJM acknowledge support from CONACyT mixed fellowships program, the DGAPA-UNAM projects IN119408 and IN106911, and the UNAM PAEP program. LC acknowledges the hospitality and support of the ORNL Fusion Energy Division during the elaboration of this work. DdCN thanks Alex Wurm for valuable discussions during the early stages of this research. DdCN was sponsored by the Oak Ridge National Laboratory, managed by UT-Battelle, LLC, for the U.S. Department of Energy under contract DE-AC05-00OR22725.

[1] D. del-Castillo-Negrete, Chaos **10**, 75 (2000).
[2] G. Boffetta, D. del-Castillo-Negrete, C. López, G. Pucacco, and A. Vulpiani, Phys. Rev. E **67**, 026224 (2003).
[3] D. del-Castillo-Negrete, Physics of Plasmas **5**, 3886 (1998).
[4] D. del-Castillo-Negrete, in *Dynamics and Thermodynamics of Systems with Long-Range Interactions*, edited by T. Dauxois, S. Ruffo, E. Arimondo, and M. Wilkens (Springer Berlin / Heidelberg, 2002), vol. 602 of *Lecture Notes in Physics*, pp. 407–436.
[5] D. del-Castillo-Negrete and P. J. Morrison, Physics of Fluids A: Fluid Dynamics **5**, 948 (1993).
[6] D. del-Castillo-Negrete and P. J. Morrison, Bull. Am. Phys. Soc. pp. 37–1543 (1992).
[7] R. Balescu, Phys. Rev. E **58**, 3781 (1998).
[8] G. A. Oda and I. Caldas, Chaos, Solitons and Fractals **5**, 15 (1995).
[9] A. Delshams and R. de la Llave, SIAM J. on Mathematical Analysis **31**, 1235 (2000).
[10] D. del-Castillo-Negrete, J. Greene, and P. Morrison, Physica D: Nonlinear Phenomena **91**, 1 (1996).
[11] I. I. Rypina, M. G. Brown, F. J. Beron-Vera, H. Koçak, M. J. Olascoaga, and I. A. Udovydchenkov, Phys. Rev. Lett. **98**, 104102 (2007).
[12] A. Wurm, A. Apte, K. Fuchss, and P. J. Morrison, Chaos **15**, 023108 (2005).
[13] S. Shinohara and Y. Aizawa, Progress of Theoretical Physics **97**, 379 (1997).
[14] B. Mandelbrot, *The fractal Geometry of Nature* (Free-man, San Francisco, 1982).
[15] J. D. Farmer, Phys. Rev. Lett. **55**, 351 (1985).
[16] N. J. Balmforth, C. Piccolo, and O. M. Umurhan, J. Fluid Mech. **449**, 115 (2001).